Article

Cell

Steroid Receptors Reprogram FoxA1 Occupancy through Dynamic Chromatin Transitions

Graphical Abstract

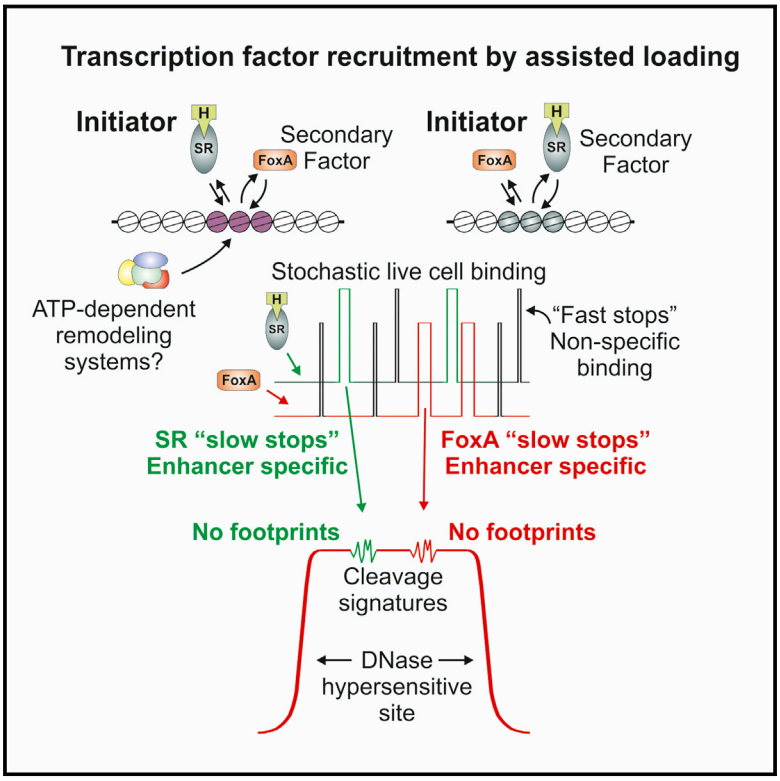

Authors

Erin E. Swinstead, Tina B. Miranda, Ville Paakinaho, ..., Lars Grøntved, Diego M. Presman, Gordon L. Hager

Correspondence

hagerg@exchange.nih.gov

In Brief

Single-molecule tracking reveals that a transcription factor, FoxA1, that has been characterized as a pioneer chromatin binder associates with DNA more dynamically than expected and that its role in promoting DNA binding of steroid receptors can in some instances be reciprocated, with the steroid receptors promoting binding of FoxA1

Highlights

- Binding patterns for the FoxA1 pioneer factor can be modulated by steroid receptors
- Interactions of FoxA1 with chromatin in live cells are highly dynamic
- The FoxA1 factor fails to produce significant footprints at chromatin-binding sites
- Redistribution of FoxA1 binding occurs through a dynamic assisted loading mechanism

Accession Numbers

GSE72252

Swinstead et al., 2016, Cell *165*, 1–13
April 21, 2016
http://dx.doi.org/10.1016/j.cell.2016.02.067

CellPress

Please cite this article in press as: Swinstead et al., Steroid Receptors Reprogram FoxA1 Occupancy through Dynamic Chromatin Transitions, Cell (2016), http://dx.doi.org/10.1016/j.cell.2016.02.067

Cell

Steroid Receptors Reprogram FoxA1 Occupancy through Dynamic Chromatin Transitions

Erin E. Swinstead,[1,4] Tina B. Miranda,[1,4] Ville Paakinaho,[1] Songjoon Baek,[1] Ido Goldstein,[1] Mary Hawkins,[1] Tatiana S. Karpova,[1] David Ball,[1] Davide Mazza,[2] Luke D. Lavis,[3] Jonathan B. Grimm,[3] Tatsuya Morisaki,[1,5] Lars Grøntved,[1,6] Diego M. Presman,[1] and Gordon L. Hager[1,*]

[1]Laboratory of Receptor Biology and Gene Expression, Building 41, 41 Library Drive, NCI, NIH, Bethesda, MD 20892, USA
[2]Istituto Scientifico Ospedale San Raffaele, Centro di Imaging Sperimentale e Università Vita-Salute San Raffaele, 20132 Milano, Italy
[3]Janelia Research Campus, Howard Hughes Medical Institute, 19700 Helix Drive, Ashburn, VA 20147, USA
[4]Co-first author
[5]Present address: Department of Biochemistry and Molecular Biology, Colorado State University, Fort Collins, CO 80523, USA
[6]Present address: Department of Biochemistry and Molecular Biology, University of Southern Denmark, 5230 Odense M, Denmark
*Correspondence: hagerg@exchange.nih.gov
http://dx.doi.org/10.1016/j.cell.2016.02.067

SUMMARY

The estrogen receptor (ER), glucocorticoid receptor (GR), and forkhead box protein 1 (FoxA1) are significant factors in breast cancer progression. FoxA1 has been implicated in establishing ER-binding patterns though its unique ability to serve as a pioneer factor. However, the molecular interplay between ER, GR, and FoxA1 requires further investigation. Here we show that ER and GR both have the ability to alter the genomic distribution of the FoxA1 pioneer factor. Single-molecule tracking experiments in live cells reveal a highly dynamic interaction of FoxA1 with chromatin in vivo. Furthermore, the FoxA1 factor is not associated with detectable footprints at its binding sites throughout the genome. These findings support a model wherein interactions between transcription factors and pioneer factors are highly dynamic. Moreover, at a subset of genomic sites, the role of pioneer can be reversed, with the steroid receptors serving to enhance binding of FoxA1.

INTRODUCTION

Pioneer factors (PFs) have been described as a class of proteins that penetrate closed chromatin to create accessible binding sites for general transcription factors (TFs) during development (Zaret and Carroll, 2011). The forkhead box protein 1 (FoxA1) has been shown to interact with compact chromatin, modulating chromatin structure as an early event. Upon chromatin binding, FoxA1 is thought to initiate nucleosome binding via the winged-helix domain that it shares with the H1 linker histone and induce nucleosomal rearrangements by a mechanism independent of ATP-dependent remodeling complexes. These transitions in turn result in an increase in the accessibility of DNA-binding elements (Bernardo and Keri, 2012; Cirillo et al., 1998, 2002). This mechanism has been widely implicated for the recruitment of steroid receptors (SRs) (Bernardo and Keri, 2012; Eeckhoute et al., 2006; He et al., 2012; Hurtado et al., 2011), specifically for the estrogen receptor (ER) and androgen receptor (AR) in breast and prostate cancer cells, respectively. Early studies reported that FoxA1-binding sites overlap with ~50% of ER-binding sites (Carroll et al., 2005) and that FoxA1 is required for at least half of all ER-binding events in MCF-7 breast cancer cells (Carroll et al., 2005; Laganière et al., 2005). Later findings via genome-wide analysis (Carroll et al., 2006; Lupien et al., 2008; Hurtado et al., 2011) have been interpreted in support of this general model. In addition, it has been reported that inhibition of ER produces no change in FoxA1 genomic binding patterns (Lupien et al., 2008; Hurtado et al., 2011). These investigations have either focused on a small number of binding locations or compared FoxA1 binding only between unstimulated cells and cells treated with an ER antagonist (Hurtado et al., 2011; Lupien et al., 2008). Contrary to these findings, an independent study reported that upon knockdown of ER, FoxA1 binding is lost at many unstimulated ER-binding sites (Caizzi et al., 2014), evidence that ER may in fact regulate binding of FoxA1.

More recently it was demonstrated that multiple TFs can modulate each other's binding patterns through a mechanism termed dynamic assisted loading. In this model, one factor can induce accessibility for another through the recruitment of ATP-dependent remodeling complexes that create transient open chromatin states (Biddie et al., 2011; Grøntved et al., 2013; Miranda et al., 2013; Voss et al., 2011), allowing the secondary factor to bind. This model is distinguished from the classic pioneering concept by three important parameters: (1) the initiating and secondary binding factors can reverse roles, depending on the local chromatin environment, (2) residence times for the binding factors are quite short, measured in seconds (s), and (3) a central role for ATP-dependent remodeling proteins is proposed (Voss and Hager, 2014; Voss et al., 2011).

Here, we show that activation of either ER or the glucocorticoid receptor (GR) induces the reprograming of the chromatin landscape in breast cancer cells and results in the recruitment of FoxA1 to a subset of sites that were previously inaccessible. In addition, we find no evidence of FoxA1, ER, or GR footprints within DNase I hypersensitive (DHS) sites in multiple breast

cancer cells. Finally, as measured by single-molecule tracking (SMT), FoxA1 manifests a highly dynamic behavior in the nucleus (comparable to that of ER and GR), with relatively fast dwell times. Together, these results suggest that these factors interact dynamically with chromatin through a symmetric mechanism. That is, the SRs can induce loading of FoxA1, or FoxA1 can reorganize nucleoprotein states consistent with receptor binding.

RESULTS

Steroid Receptors Can Modulate the Binding Patterns of FoxA1

We reported recently that ER and GR can facilitate the binding of one another at a subset of binding sites, suggesting that ER and GR have the ability to function as initiating factors for each other (Miranda et al., 2013). To further investigate the "pioneering mechanism" of FoxA1, ER, and GR, we mapped the binding profiles for FoxA1 following activation of ER or GR in MCF-7, ZR-75-1, and T-47D breast cancer cell lines, three of the most commonly studied, estrogen-responsive breast cancer models (Lacroix and Leclercq, 2004). Analysis of the direct overlap between FoxA1- and ER-binding patterns and FoxA1- and GR-binding patterns revealed a number of unique clusters (denoted by lowercase letters). For FoxA1-binding sites identified in unstimulated and 17β-estradiol (E2) treated MCF-7 cells, a large proportion (~80%) appear to have no close-range proximity to ER-binding sites (Figure 1A, clusters "a," "b," and "c"). For all ER sites stimulated by E2 treatment, 44% overlap with FoxA1 sites active in unstimulated cells and E2-treated cells (cluster "e"). A lesser yet significant proportion (~14%) of ER-binding sites overlap with FoxA1 sites functional only in E2-stimulated cells (cluster "f") with only ~0.8% of ER sites overlapping with unstimulated FoxA1 sites in the absence of E2 (cluster "g"). The individual binding intensities of the FoxA1 and ER peaks have been compared via heatmap analysis, indicating the presence or absence of FoxA1 and ER binding at each binding group described by the Venn diagram (denoted by lowercase letters; Figure 1C). The locations of the FoxA1 and ER peaks and the average tag count have been presented for each of the three significant binding groups by aggregate plots, confirming the uniqueness of each binding group (Figure 1E). These findings indicate that the relationship between FoxA1 and ER is more complex than previously reported.

The interaction between FoxA1 and GR in breast cancer cells has not been comprehensively explored. In fact, ~69% of dexamethasone (Dex) inducible GR sites overlap with FoxA1 sites present in unstimulated and Dex-treated cells (Figure 1B, cluster "l"), suggesting that FoxA1 plays a significant role in GR recruitment. A large fraction of FoxA1 sites (~77%) are unrelated to GR binding (clusters "h," "j," and "i"). Seventeen percent of GR sites have no overlap with FoxA1 binding (cluster "k"), and a smaller number (~12%) overlap with FoxA1 that is bound only in Dex-stimulated cells (Figure 1B, cluster "m"). Heatmap analysis (Figure 1D) presents individual intensities for FoxA1 and GR for the binding groups denoted by lowercase letters. The average tag count and binding location of GR and FoxA1 are shown via histogram (Figure 1F). Thus the hormone-activated differences in FoxA1 genome-wide occupancy are similar between GR and ER. Analysis of FoxA1, ER, and GR binding in ZR-75-1 (Figures S1A and S1B) and T-47D (Figures S1C and S1D) cells presents similar findings, supporting the results identified in MCF-7 cells.

Of particular interest is the subset of ER- and GR-binding sites that overlap with FoxA1 only after hormone stimulation ("f" and "m"), as well as the FoxA1 population of binding sites altered by hormone treatment yet not overlapping with an SR site ("a" and "h"). These classes represent sites where ER and GR serve as initiating factors for FoxA1. To investigate this observation further we first determined, genome-wide, the binding locations and distances between all FoxA1 and ER peaks (Figures 2A and 2B) and all FoxA1 and GR peaks (Figures 2C and 2D). We combined all FoxA1-binding sites identified in untreated and E2 samples and untreated and Dex samples. The cumulative distribution of FoxA1 peaks to the closest ER-binding event (broken line) and closest estrogen response element (ERE) motif (solid line) has been determined at a range of 0–500 base pairs (bp) (Figure 2A) and 0–10,000 bp (Figure 2B). This distribution was also determined for all FoxA1 peaks in relation to the closest GR-binding event (broken line) and the closest glucocorticoid response element (GRE) motif (solid line) at a range of 0–500 bp (Figure 2C) and 0–10,000 bp (Figure 2D). Less than 5% of all FoxA1 peaks are located within 100 bp of an ERE motif, and ~15% are located within 100 bp of an ER peak (Figure 2A). Furthermore, only 2.5% of FoxA1 peaks are within 100 bp of a GRE motif, and ~20% are within 100 bp of a GR peak (Figure 2C). These close-range binding classes represent events wherein potential localized nucleosome reorganization by FoxA1 could lead directly to SR binding. However at longer ranges, only ~30% and ~25% of FoxA1 peaks are located within 10,000 bp of an ER peak (Figure 2B) or a GR peak (Figure 2D), respectively. In addition, ~80% of FoxA1 peaks are located within 10,000 bp of the closest ERE motif (Figure 2B), and ~55% within 10,000 bp of the closest GRE motif (Figure 2D), indicating that there are many unbound ERE and GRE motifs within 10,000 bp of a FoxA1 peak. These findings are quite unexpected, given the widely described behavior of FoxA1 as a PF for SR function.

A large number of ER and GR sites pioneered by FoxA1 lack a binding interaction and SR motif within 100 bp. To look more closely at this observation, we examined the FoxA1 peaks identified in the Venn diagrams in Figure 1. Specifically we used the ER and GR peaks that overlap with FoxA1 peaks present only in hormone-treated cells ("f" and "m"), ER and GR peaks that overlap with FoxA1 in unstimulated and hormone-treated cells (classically considered to be ER and GR peaks pioneered by FoxA1 ["e" and "l"]), and FoxA1 peaks unique to hormone treatment in the absence of an ER or GR peak ("a" and ""h") (Figures 2E and 2F). Of the classical pioneer FoxA1 sites for ER ("e"), ~90% are located within 100 bp of an ER peak (Figure 2E), and for classical pioneer FoxA1 sites for GR ("l"), ~93% are located within 100 bp of a GR peak (Figure 2F). Therefore of the small number of FoxA1 sites (~15%–20%) that function as a PF for either ER or GR, ~90% are located within 100 bp of an ER or GR peak. However, an important observation is that FoxA1 peaks overlapping ER and GR in the hormone-treated groups only ("f" and "m") have a higher percentage (95% and 97%, respectively) located within 100 bp of an ER or GR peak (Figures 2E and 2F). Further, approximately 60% of these peaks

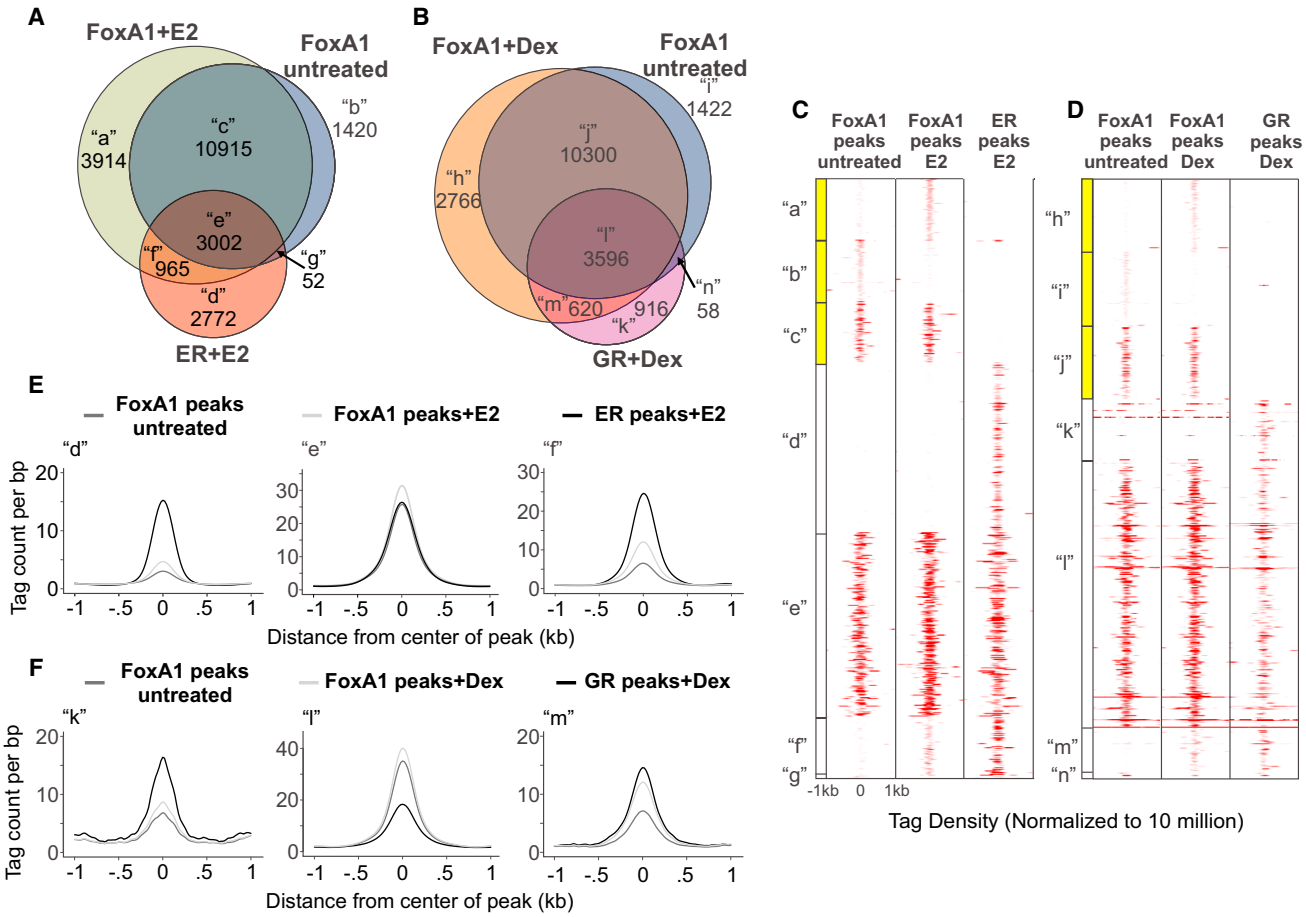

Figure 1. Binding Patterns of FoxA1, ER, and GR in Hormone-Treated MCF-7 Breast Cancer Cells

ChIP-seq binding profiles are shown for ER, GR, and FoxA1 for untreated cells or cells treated with E2 or Dex.

(A) Venn diagram represents the number of ER+E2-binding sites that overlap with FoxA1+E2- or FoxA1 untreated-binding sites.

(B) Venn diagram demonstrates the overlap of ChIP-seq GR+Dex-induced binding patterns with FoxA1+Dex- and FoxA1 untreated-binding patterns. Each group identified has been notated with a lowercase letter.

(C) Heatmap represents the binding intensity of FoxA1 untreated, FoxA1+E2, and ER+E2 at the specific binding groups characterized by the Venn diagram and labeled by lowercase letters. The heatmap is presented as the number of reads per 10^6 sequences with the position of the reads in a 2 kb region flanking the center of the peak. Groups "a," "b," and "c" are examples of 1,000 binding sites from the individual groups and are highlighted in yellow.

(D) The heatmap represents the ChIP-seq tag density of FoxA1 untreated, FoxA1+Dex, and GR+Dex peaks at the binding patterns identified in the Venn diagram and labeled by a lowercase letter. The heatmap is presented as the number of reads per 10^6 sequences with the position of the reads in a 2 kb region flanking the center of the peak. Groups "h," "i," and "j" are an example of 1,000 binding sites from the individual groups and are highlighted in yellow.

(E) Three histograms represent the average tag count of all ER+E2 ChIP-seq samples, FoxA1 untreated ChIP-seq samples, and FoxA1+E2 ChIP-seq samples at the specific binding groups of "d," "e," and "f" over a 2 kb region.

(F) The three histograms represent the average tag count of all FoxA1 untreated, FoxA1+Dex, and GR+Dex ChIP-seq samples over a 2 kb distance for sites identified at groups "k," "l," and "m."

See also Figure S1.

are within 10 bp of an ER or GR peak compared to only ~35% of the observed classical FoxA1 peaks known to pioneer for ER or GR ("e" and "l") (insets in Figures 2E and 2F). These findings suggest that there are populations of FoxA1 peaks regulated by hormone and in close proximity to the regulating TF, which signifies that ER or GR have the potential to recruit FoxA1 to binding locations.

To investigate the potential hormone regulation of FoxA1-binding pattern, we further analyzed the FoxA1, ER, and GR chromatin immunoprecipitation sequencing (ChIP-seq) data to determine the differential hormone regulation of FoxA1. This analysis of FoxA1-binding sites shows that ER and GR can also recruit FoxA1 to a subset of specific sites in MCF-7, ZR-75-1, and T-47D cells (ZR-75-1 and T-47D; Figures S2A and S2B). In MCF-7 cells there are 19,068 FoxA1-binding sites found to be in common with untreated and E2-treated cells and 1,219 binding sites that are gained or lost upon E2 stimulation (Figure 2G). Of the total FoxA1-binding sites identified in cells treated with Dex or left untreated, 18,142 are found to occur in both treatment conditions, with 571 FoxA1 sites gained and 72 lost

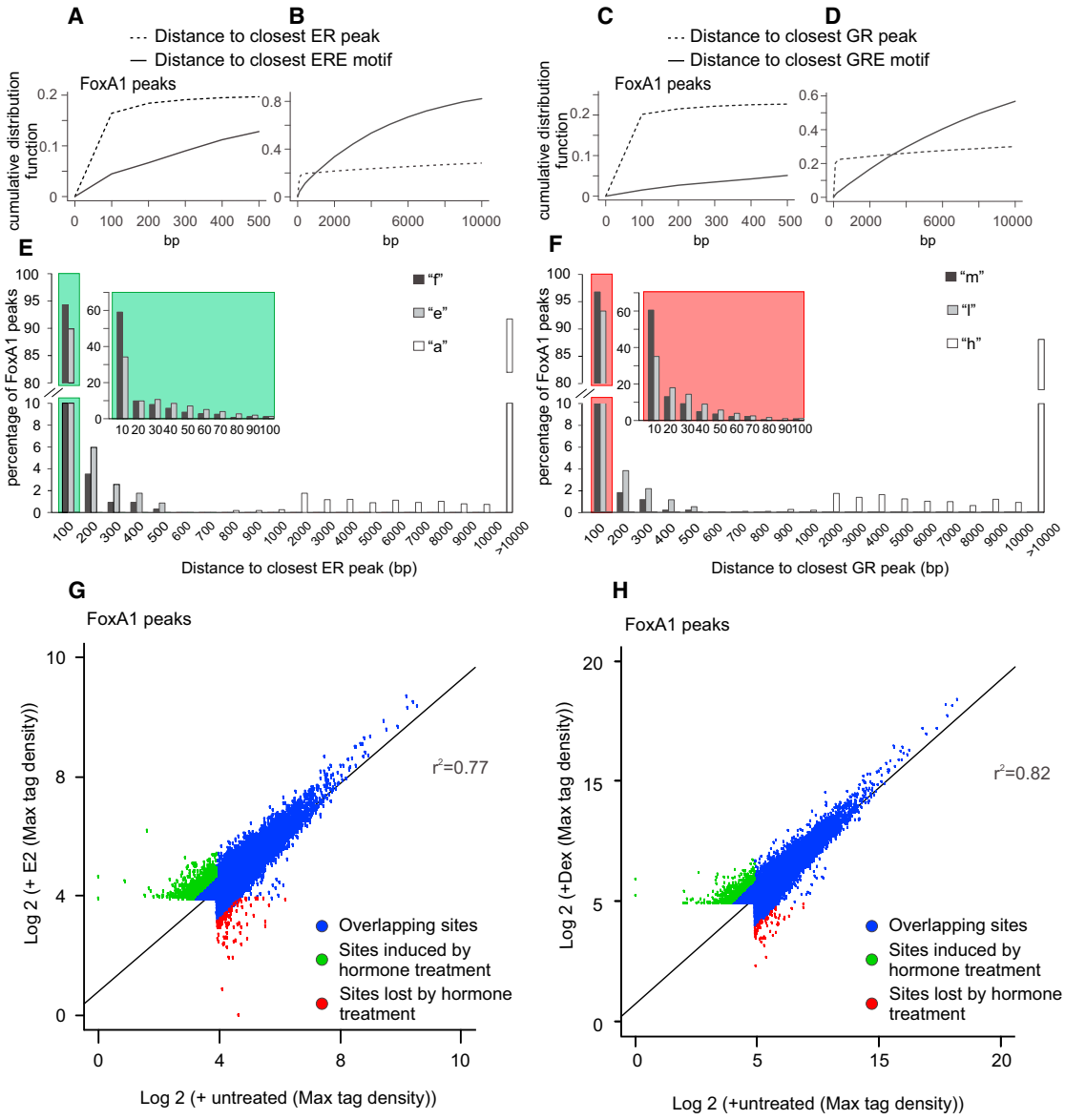

Figure 2. Positioning Analysis and Differential Hormone Regulation of FoxA1 in MCF-7 Breast Cancer Cells

The average location of FoxA1 in relation to ER and GR peaks over a 10 kb range.

(A and B) Cumulative distribution function plotted to determine the location of all FoxA1 (untreated and E2-treated) sites in relation to all ER+E2-binding sites (broken line) and ERE motif (solid line) over a 500 bp range (A) and 10 kb range (B).

(C and D) The distances of all FoxA1 (untreated and Dex) peaks in relation to GR+Dex-binding sites (broken line) and GRE motif (solid line) over a 500 bp range (C) and 10 kb rang (D) have been plotted as a cumulative distribution function.

(E) The percentage of FoxA1 peaks within a 10 kb range of the closest ER peak is shown. FoxA1 sites are identified in groups "f" (black), "e" (gray), and "a" (white). Expanded view shows the percentage of FoxA1 peaks within a 100 bp range of the closest ER peak.

(F) The percentage of FoxA1 peaks closest to a GR peak within a 10 kb distance has been calculated and separated into sites identified in the individual binding groups for "m" (black), "l" (gray), and "h" (white).(Expanded view) The distance has been decreased to 100 bp and the percentage calculated for sites identified in individual groups.

(G) Scatterplot shows the genome-wide changes in FoxA1 binding in untreated compared with E2-treated cells. Green points denote sites induced by E2, red points denote sites lost by E2, and blue points denote sites unchanged by E2 treatment. Sites gained or lost by E2 have a 2-fold change in tag density over the background of the E2 treatment.

(H) The genome-wide changes in FoxA1 binding in untreated compared with Dex-treated cells are displayed in the scatterplot. Green points denote sites induced with Dex, red points denote sites lost by Dex, and blue points denote sites unchanged with Dex. Sites gained or lost by Dex have a 2-fold change in tag density over the background of the Dex treatment.

See also Figure S2.

with Dex treatment (Figure 2H). This demonstrates that activated ER and GR have the ability to re-distribute the binding patterns of FoxA1, consistent with a previous report whereby the dual activation of ER and GR reprograms the binding landscape through the gain and loss of binding sites (Miranda et al., 2013). Together these results suggest that FoxA1, ER, and GR in breast cancer cell lines each have the capability of altering a subset of binding sites, reinforcing the notion that multiple factors can function in a ''pioneering'' mode.

ER and GR Can Function in an Assisted Loading Mechanism by Inducing FoxA1-Binding Sites

To further define the specific role of each receptor in redistributing FoxA1 binding across the genome, supervised clustering analysis of FoxA1, ER, and GR ChIP-seq data in each cell line has been performed to extract specific binding modules. In MCF-7 cells three unique binding clusters have been identified for FoxA1 and ER sites induced and lost by E2 (Figures 3A and 3B). Cluster 1 (122 peaks) represents FoxA1 sites that are lost upon E2 treatment and do not overlap with ER binding. Cluster 2 (625 peaks) includes FoxA1 sites that are gained by E2 treatment but do not overlap with ER-binding sites. The lack of overlap with ER at cluster 2 suggests that FoxA1 binding at these sites is either through a tethering interaction or a representation of a hit-and-run event (McNally et al., 2000; Hager et al., 2002) whereby ER is binding with such a short residence time that a ChIP signal is not detected. Lastly, cluster 3 represents unique sites wherein FoxA1 binding is gained with E2 treatment only and overlaps with ER-binding sites (470 peaks), suggesting that ER activation may result in ER-induced FoxA1 sites through assisted loading.

In addition, four FoxA1- and GR-binding clusters have been identified (Figures 3D and 3E). Specifically, cluster 1 (236 peaks) represents FoxA1 sites gained with Dex treatment and overlap with GR-binding sites. This cluster also demonstrates that GR activation may recruit FoxA1 to specific sites through a GR-induced mechanism (GR-induced FoxA1 sites). Cluster 2 (335 peaks) represents FoxA1-binding sites that are gained with Dex treatment and that do not overlap with GR-binding sites, again suggesting a potential hit-and-run event for FoxA1 recruitment. Cluster 3 (16 peaks) represents FoxA1 sites that are lost upon Dex treatment and that overlap with GR sites. Cluster 4 also contains FoxA1 lost sites (56 peaks); however, these peaks do not overlap with GR-binding sites. Supervised clustering analysis of ZR-75-1 cells (Figures S3A and S3B) and T-47D cells (Figures S3C and S3D) for ER, GR, and FoxA1 reveals very similar binding patterns.

Interestingly, the specific ER- and GR-induced FoxA1 sites identified in the three cell lines reveal very little overlap, suggesting that although the mechanism of assisted loading is active in breast cancer cells, the binding sites are cell line specific (Figures S3E and S3F). This indicates that different types of breast cancer may have an altered assisted loading binding pattern. It has previously been demonstrated that a number of FoxA1- and ER-binding sites are cell line specific in MCF-7, ZR-75-1, and T-47D cells (Hurtado et al., 2011). This supports the concept that multiple TF-binding sites can be largely unique to individual cell lines.

To further examine the direct role of ER and GR on dictating FoxA1 binding at the induced sites identified in MCF-7 cells, de novo motif analysis has been performed. At ER-induced FoxA1 sites there is a strong ERE and a weaker FoxA1 motif. In contrast, at FoxA1 classical binding sites observed in both the untreated or E2-treated cells, the FoxA1-binding element is the most highly enriched motif (Figure 3C). At the GR-induced FoxA1 sites a GRE element is the most highly enriched motif, and there is a weak FoxA1 motif (comparable to that at the ER-induced FoxA1 sites). At FoxA1 classical sites observed in the untreated and Dex-treated cells, the FoxA1 motif is highly prevalent (Figure 3F). Thus, although FoxA1 binding can be modulated by activation of SRs through an assisted loading mechanism, FoxA1 also dictates ER and GR binding at a small set of FoxA1-specific sites. In addition, there is an AP-1 motif identified at the ER- and GR-induced FoxA1-binding sites, suggesting that AP-1 might be playing a functional role with SRs to assist the loading of FoxA1. This supports previous findings that AP-1 is a required component of GR binding at 40% of binding sites (Biddie et al., 2011). Further, it has also been identified that AP-1 is required for GR-induced binding of ER sites (Miranda et al., 2013). Together these findings demonstrate that ER and GR, in collaboration with factors such as AP-1, have the ability to reshape the FoxA1-binding landscape and frequently act as initiating factors for FoxA1.

DNase Hypersensitivity Increases at ER- and GR-Induced FoxA1 Sites

To further understand the chromatin landscape of sites identified at the SR-induced FoxA1 sites, we performed DHS-seq analysis in MCF-7 and ZR-75-1 cells under E2 or Dex treatment and characterized the change in DHS at all identified clusters in both cell lines (Figures 4 and S4). In MCF-7 cells at ER-induced FoxA1 sites (cluster 3), there is an increase in DHS upon E2 treatment (Figure 4A). The same pattern is observed in chromatin accessibility at GR-induced FoxA1 sites (Figure 4B). These same results are also observed at the clusters identified in ZR-75-1 cells (Figures S4A and S4B). Of particular note, FoxA1 sites that are activated with E2 or Dex and do not overlap with SR binding (cluster 2) are also remodeled, indicating that despite the absence in binding the receptor is involved, either by hit-and-run or by tethering, in chromatin remodeling. Examples of specific binding locations are shown as UCSC browser shots for ER-induced FoxA1 sites (Figure 4A) and GR-induced FoxA1 sites (Figure 4B).

Our results from multiple cell lines demonstrate that although the specific binding sites have unique cell specificity, the assisted loading mechanism is functional in breast cancer cells through ER and GR modulation of FoxA1-binding patterns. Thus ER and GR, much like FoxA1 (Hurtado et al., 2011), can cause changes in chromatin accessibility allowing for the recruitment of other TFs to specific response elements.

FoxA1 Does Not Present a DNase Footprint and Binds Transiently to DNA

When occupied by their cognate factor, TF-binding sites on DNA are resistant to nuclease digestion and can be monitored by the generation of a TF footprint (Galas and Schmitz, 1978). Similar

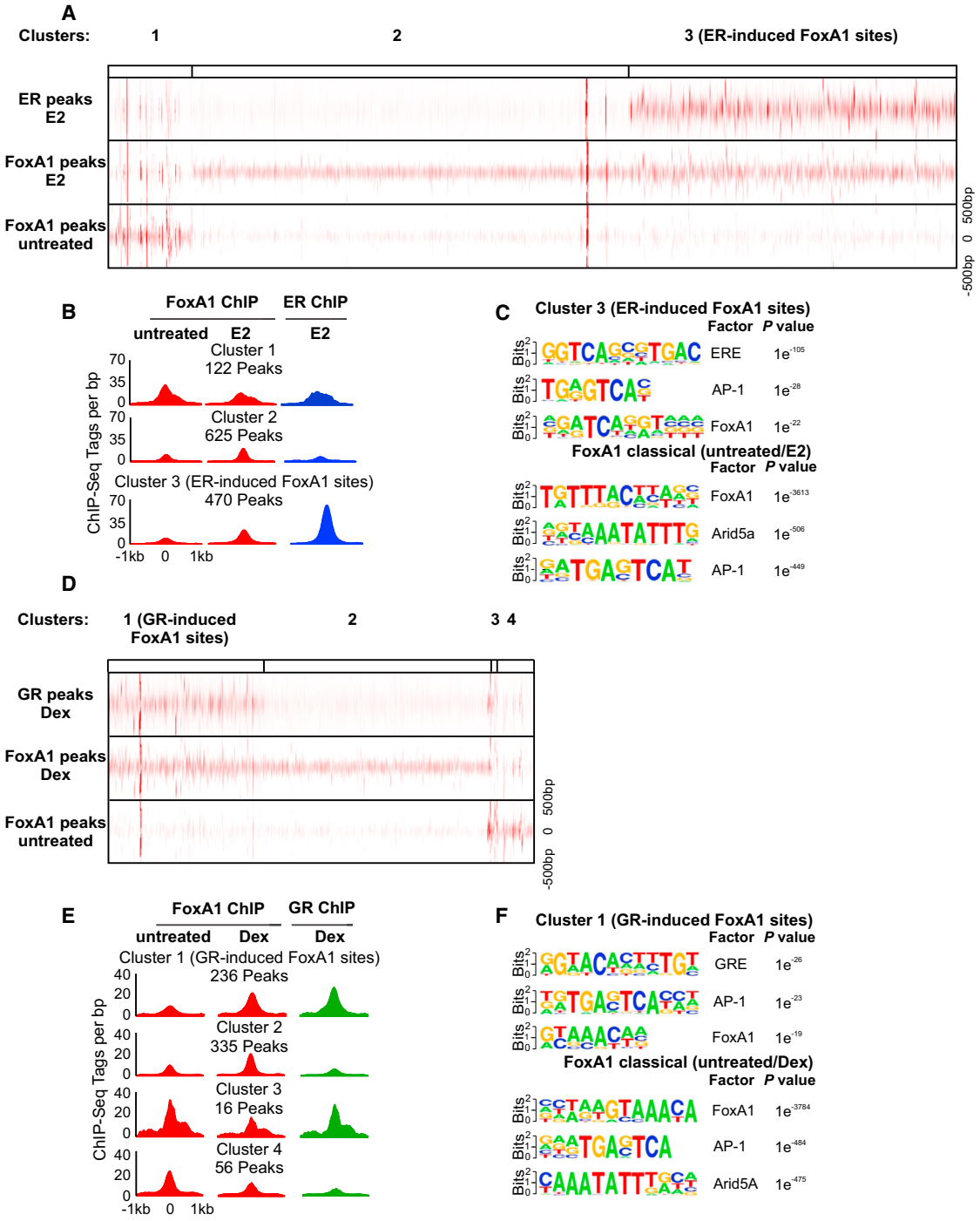

Figure 3. Supervised Clustering Analysis Reveals Different FoxA1-Binding Modules in MCF-7 Cells

(A) Supervised cluster analysis of ER-binding sites and FoxA1-binding patterns found to be gained or lost with E2 treatment with a 2-fold change in tag density reveals three specific clusters with cluster 3 representing ER-induced FoxA1 sites. The heatmap represents the number of reads per 10^6 sequences and the position of the reads in a 1 kb region flanking the peak.

(B) Histogram represents the average tag count per bp over a 2 kb range of FoxA1 and ER at the three identified clusters.

(C) De novo motif analysis has been conducted on sites identified as ER-induced FoxA1 sites and compared to the FoxA1 classical cluster omitted from the supervised clustering analysis.

(legend continued on next page)

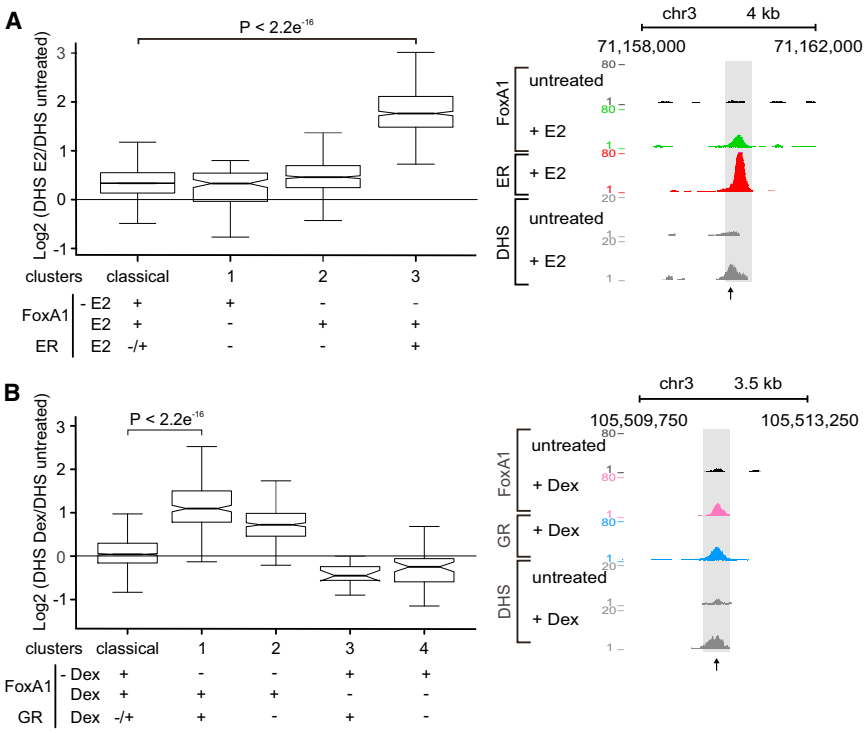

Figure 4. Chromatin Accessibility Altered at Hormone-Induced FoxA1-Binding Sites

(A) Boxplot analysis comparing cells treated with E2 or left untreated show that there are significant changes in DHS at the ER-induced FoxA1 sites (cluster 3) compared with the FoxA1 classical cluster. Genomic region illustrating changes in DHS at a specific ER-induced FoxA1 site (UCSC browser shot) is shown.

(B) Analysis of DHS-seq in cells either treated with Dex or left untreated demonstrates a significant increase in chromatin remodeling at GR-induced FoxA1 sites (cluster 1) compared with the FoxA1 classical cluster. A genomic region identified at a GR-induced FoxA1 site illustrates changes in DHS (UCSC browser shot). p values are determined by the two-sample Kolmogorov Smirnov test.

See also Figure S4.

patterns of protection have been identified in nuclease-digested nuclei (Church et al., 1985) and are often inferred to represent stable binding of a factor at the recognition site. This interpretation of a footprint profile fundamentally conflicts with many studies showing very brief residence times for DNA-binding proteins in living cells (Voss and Hager, 2014). Furthermore, it has been recently reported that factors with robust ChIP-seq peaks but short DNA residence times in live cells manifest either a minimal or complete lack of a footprint in vivo (Sung et al., 2014; He et al., 2014; Grøntved et al., 2015).

FoxA1 has been considered a master PF and has been argued to present stable DNA interactions with low mobility (Caravaca et al., 2013; Sekiya et al., 2009), in contrast with the dynamic function of a number of TFs. To characterize FoxA1, ER, and GR intranuclear dynamics, we performed SMT for these factors (Movies S1, S2, S3, S4, S5, and S6). We used HaloTag and Janelia Fluor 549 (JF_{549}) HaloTag ligand versions of FoxA1, ER, and GR expressed in MCF-7 cells to identify and track single molecules with highly inclined laminated optical sheet (HILO) illumination (Tokunaga et al., 2008). We observed three dwell time classes for FoxA1, ER, and GR molecules (Figure 5), unbound, fast, and slow. Quantitative analysis of large track sets (Figures S5A–S5F) shows that the dwell-time distributions fit a double-component exponential decay model for all three TFs (Figures S5G–S5L), indicating the presence of two distinct bound-populations. The lifetimes of bound factor molecules resolve into short- and longer-lived populations, referred to as fast short-lived (T_{ns}, fast) or slow long-lived (T_s, slow) fractions, respectively. Previous reports suggest that the slow long-lived population of molecules represents specific binding events associated with enhancers or promoters, whereas the fast short-lived class describes non-specific binding to chromatin (Morisaki et al., 2014). Interestingly, FoxA1 presents characteristic residence times of 1.78 ± 0.03 s at the fast short-lived fraction and 10.8 ± 0.5 s at the slow long-lived fraction in the untreated state (Figures 5A and S5A). This relatively fast dwell time of FoxA1, especially at specific binding sites, is inconsistent with a stable binding model for the FoxA1 factor. ER or GR activation leads to a modest yet significant modulation of the FoxA1 slow long-lived fractions, to 8.4 ± 0.3 s and 8.8 ± 0.6 s, respectively (Figures 5B, 5C, S5B, and S5C). Thus activation of either SR slightly decreases the stability, on average, of FoxA1 binding to chromatin. The mean residence times that we measure reflect the average of residence times for FoxA1 at all endogenous response elements, including FoxA1 sites not associated with ER- or GR-assisted loading.

The residence times of both ER and GR were found to be comparable to that of FoxA1. Without hormone stimulation, ER presents two distinct bound populations of molecules with a fast short-lived fraction and slow long-lived fraction of 0.81 ± 0.01 s and 4.4 ± 0.2 s, respectively (Figures 5D and S5D), suggesting some specific binding events to chromatin in a ligand-independent manner. This finding is consistent with studies indicating

(D) Supervised clustering analysis of GR+Dex peaks and FoxA1 untreated and Dex peaks at FoxA1 sites gained or lost by Dex treatment reveals four specific clusters with cluster 1 representing GR-induced FoxA1 sites. The heatmap represents the number of reads per 10^6 sequences and the position of the reads in a 1 kb region flanking the peak.

(E) Histogram represents the average tag count per bp over a 2 kb range of FoxA1 and GR at the four identified clusters.

(F) De novo motif analysis for sites identified as GR-induced FoxA1 sites is compared to that of the FoxA1 classical cluster.

See also Figure S3.

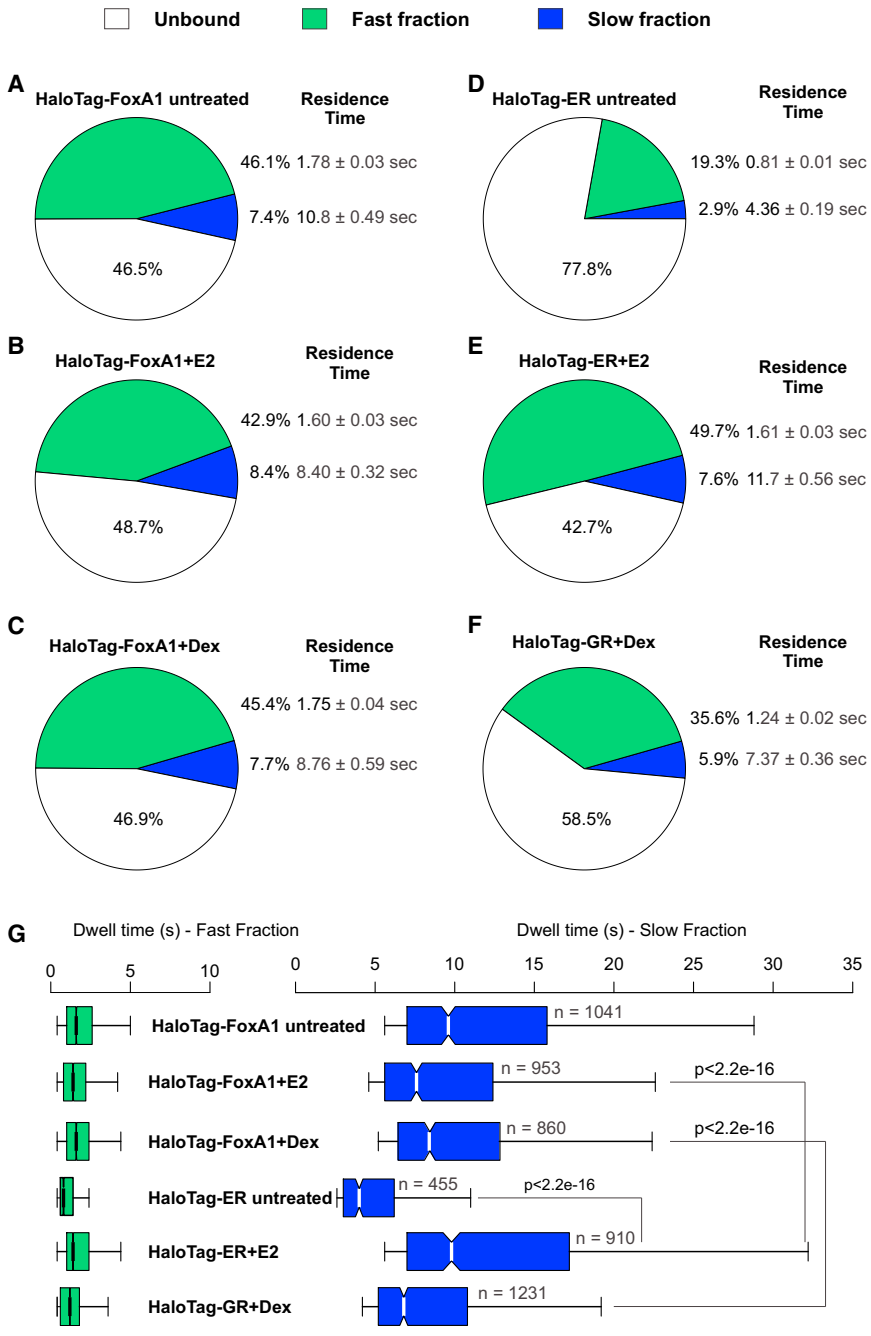

Figure 5. Single-Molecule Imaging Analysis Demonstrates a Short Residence Time for FoxA1 under All Treatment Conditions

(A–F) Top panel represents the bound fractions and the average residence time for FoxA1 in (A) untreated cells, (B) E2-treated cells, and (C) Dex-treated cells; for ER in (D) untreated cells and (E) E2-treated cells; and for GR in (F) Dex-treated cells. Pie charts (A–F) represent percentage of molecules unbound (white), bound at the fast short-lived fraction (green), and bound at the slow long-lived fraction (blue). The average residence times of fast short-lived and slow long-lived fractions are presented next to their representative fractions.

(G) Boxplot represents the dwell times for all molecules in the fast short-lived fraction (green box) and the slow long-lived fraction (blue box) for FoxA1 in untreated, E2-treated, and Dex-treated cells; for ER in untreated and E2-treated cells; and for GR in Dex-treated cells. The number of molecules in the long-lived fraction is presented as n. p value represents a two-sample Kolmogorov Smirnov test defined by the brackets.

See also Figure S5.

that there are subsets of functional ER-binding sites in the unliganded state in MCF-7 cells (Caizzi et al., 2014; Kong et al., 2011). Upon activation of ER, the residence time at the slow long-lived fraction is increased significantly, averaging 11.7 ± 0.6 s (Figures 5E and S5E). In addition, the percentage of ER molecules in the slow long-lived fraction is markedly increased (Figures 5D and 5E), consistent with increased site-specific binding for the receptor after ligand activation. GR manifests residence times of 1.24 ± 0.02 s and 7.4 ± 0.4 s in the Dex-treated state (Figures 5F and S5F), similar to previous reports (Morisaki et al., 2014). Interestingly, although FoxA1 is significantly slower than GR+Dex complexes, ER+E2 is significantly slower than FoxA1 (Figure 5G). Furthermore, comparison of FoxA1, ER, and GR indicates that activated ER shows the slowest residence time of the three factors. Thus, the SMT data do not support a stable model of FoxA1 DNA binding but rather indicate that FoxA1, like ER and GR (Figure 5G), is highly dynamic with relatively fast DNA residence times.

The question is now raised as to whether the binding events of FoxA1 can provide protection for its binding sites as detected by footprint analysis. An example of a well-described footprint is shown for the CTCF protein, a transcriptional repressor, in MCF-7 untreated cells (Figure S6A). As previously described, this deep footprint correlates with a relatively slow DNA residence time for the CTCF factor (Boyle et al., 2011; Nakahashi et al., 2013; Siersbæk et al., 2014; Sung et al., 2014). On the contrary, in MCF-7 cells there is no genome-wide FoxA1 footprint detected in the untreated, E2-treated, or Dex-treated samples (Figures 6A–6C). This finding is also observed in ZR-75-1 cells (Figures S6B–S6D). Furthermore, in E2- and Dex-treated samples we observe the lack of a detectable ER or GR footprint in MCF-7 and ZR-75-1 cells, respectively (Figures 6D, 6E, S6E, and S6F), which supports previous studies (Sung et al., 2014). Furthermore, the ability to detect a FoxA1 footprint is not changed subject to protein-binding intensity with the bottom 2,000 and top 500 FoxA1 peaks not altering the outcome

of footprint detection (Figures S6G and S6H). The footprint data, in conjunction with the SMT findings, indicate that FoxA1, like ER and GR, is a highly dynamic TF. This contrasts with previous models for FoxA1 interactions with chromatin, wherein FoxA1 is hypothesized to penetrate inaccessible chromatin in conjunction with nucleosomes and function as a PF through stable interactions with chromatin. These dynamic properties of FoxA1 indicate that the factor is not stably bound to chromatin with a slow mobility and support a model wherein FoxA1, like GR and ER, is reprogrammable in the chromatin context.

DISCUSSION

FoxA1 has been widely discussed as a PF for SR recruitment to specific sites across the genome (Bernardo and Keri, 2012). Importantly, the interaction between FoxA1 and ER has been shown to be a prominent factor in breast cancer development (Yamaguchi et al., 2008). Several studies have argued that FoxA1 is a vital component for ER recruitment at the majority of sites in breast cancer cells (Carroll et al., 2006; Hurtado et al., 2011; Lupien et al., 2008). It is also been reported that upon inhibition of ER, no change in FoxA1 binding is observed (Lupien et al., 2008; Hurtado et al., 2011). These models envisage FoxA1 as an asymmetric PF that establishes the binding landscape for ER, whereas ER plays no role in FoxA1 binding and recruitment to chromatin. However, other studies, inconsistent with these findings, reported that FoxA1 recruitment is dependent on stimulation of cells with E2 at 29% of sites where both ER and FoxA1 bind, although no mechanism was determined (Kong et al., 2011). In addition, it was reported that upon knockdown of ER, FoxA1 binding is lost at unstimulated ER-binding sites (Caizzi et al., 2014).

SRs have also been shown to modify the binding landscape for each other. As an example, ER and GR can each act as initiating factors for binding of the other in mammary cells (Miranda et al., 2013). Furthermore, an early report (Rigaud et al., 1991) found that GR could modulate FoxA1 binding at a specific GRE within the GR-responsive unit of the rat tyrosine aminotransferase gene. This enhanced binding of FoxA1 was associated with GR-dependent disruption of nucleosomal structure and suggests that the role of SRs in the regulation of FoxA1 responses is not well understood.

Alternative mechanisms have been suggested for the "pioneering" action of TFs. AP-1 was shown to be necessary for opening chromatin at 40% of GR binding in mammary cells (Biddie et al., 2011). However, at a smaller number of sites in the same cells, GR serves as an initiating factor for AP-1 binding. Finally, at some sites, the initiating factor cannot be co-resident with the secondary loaded factor (Voss et al., 2011; Rigaud et al., 1991). Taken together, these findings suggest a more dynamic and symmetric model for the pioneering action of these factors, a mechanism that has been termed "dynamic assisted loading" (Voss et al., 2011).

The confusing and contradictory findings led us to examine the pioneering roles of these proteins in more detail. Interactions between FoxA1 and SRs were characterized here with multiple methodologies. Global ChIP-seq analysis reveals that a significant fraction of FoxA1-binding events are dependent on either GR or ER, in agreement with Kong et al. and Caizzi et al. Furthermore, each of the receptors was found to initiate chromatin opening, as determined by DNase I hypersensitivity, at sites where FoxA1 loading is dependent on the SR. Furthermore, these sites tend to contain a weaker FoxA1 motif, suggesting that after ER or GR induction, FoxA1-binding intensity changes reflecting transient FoxA1 and DNA interactions. These results indicate that the SRs have the potential to bind chromatin and recruit remodelers to make the sites more accessible, allowing for the secondary loading of FoxA1 at these sites.

If FoxA1 is bound stably to chromatin in the classic wedging model, it would be expected to produce a footprint of protection at pioneering sites. However, TFs that are highly dynamic, with rapid chromatin-exchange rates, have been shown to lack a nuclease-resistant footprint (He et al., 2014; Sung et al., 2014). ER and GR each display highly dynamic binding events with a short residence time on chromatin (McNally et al., 2000; Stenoien et al., 2001). As shown here, FoxA1 also fails to manifest a detectable footprint at binding sites, either SR dependent or independent, in the genome. The relatively fast residence times measured by the SMT experiments indicate that the binding of FoxA1 is also a highly dynamic process, with rapid FoxA1 exchange at sites in chromatin. Another PF, SOX2, was recently shown to present a transient interaction with chromatin, on the order of 12–14 s (Chen et al., 2014). These findings again support the concept of PFs as highly mobile during functional enhancer interactions.

Finally, we note that the discussion of pioneer protein function has centered almost exclusively on potential interactions between TFs and nucleosomes. In fact, where examined in detail, localized chromatin transitions are often associated with the action of ATP-dependent remodeling complexes (Mellor, 2006; Yoo and Crabtree, 2009). Several reports have shown that factors can be mobile during these remodeling processes (Kassabov et al., 2002; McKnight et al., 2011; Nagaich et al., 2004). A recent study by Wang and colleagues (Li et al., 2015) elegantly demonstrated that the Swi/Snf complex can directly displace a bound TF, supporting previous suggestions for factor mobility during remodeling. As it is well established that SRs recruit remodeling proteins, the action of these complexes in the symmetric recruitment described here requires further attention. It is possible that ATP-dependent remodeling systems are more centrally involved in pioneering factor action than previously appreciated. To seek further clarification of the direct role of ER and GR in the assisted loading mechanism, future studies involving mutation of the SR DNA-binding domain or direct mutation of the FoxA1-binding site could be performed. This would determine whether the SRs bind to their cognate site, directly facilitating FoxA1 binding. In conclusion, the results presented here support a symmetric model wherein multiple TFs can serve a pioneering function, largely dependent on the local chromatin structure at a given site. In addition, PFs FoxA1 and SOX2 each manifest highly dynamic interactions with chromatin, with exchange rates comparable to those for SRs and other highly mobile factors.

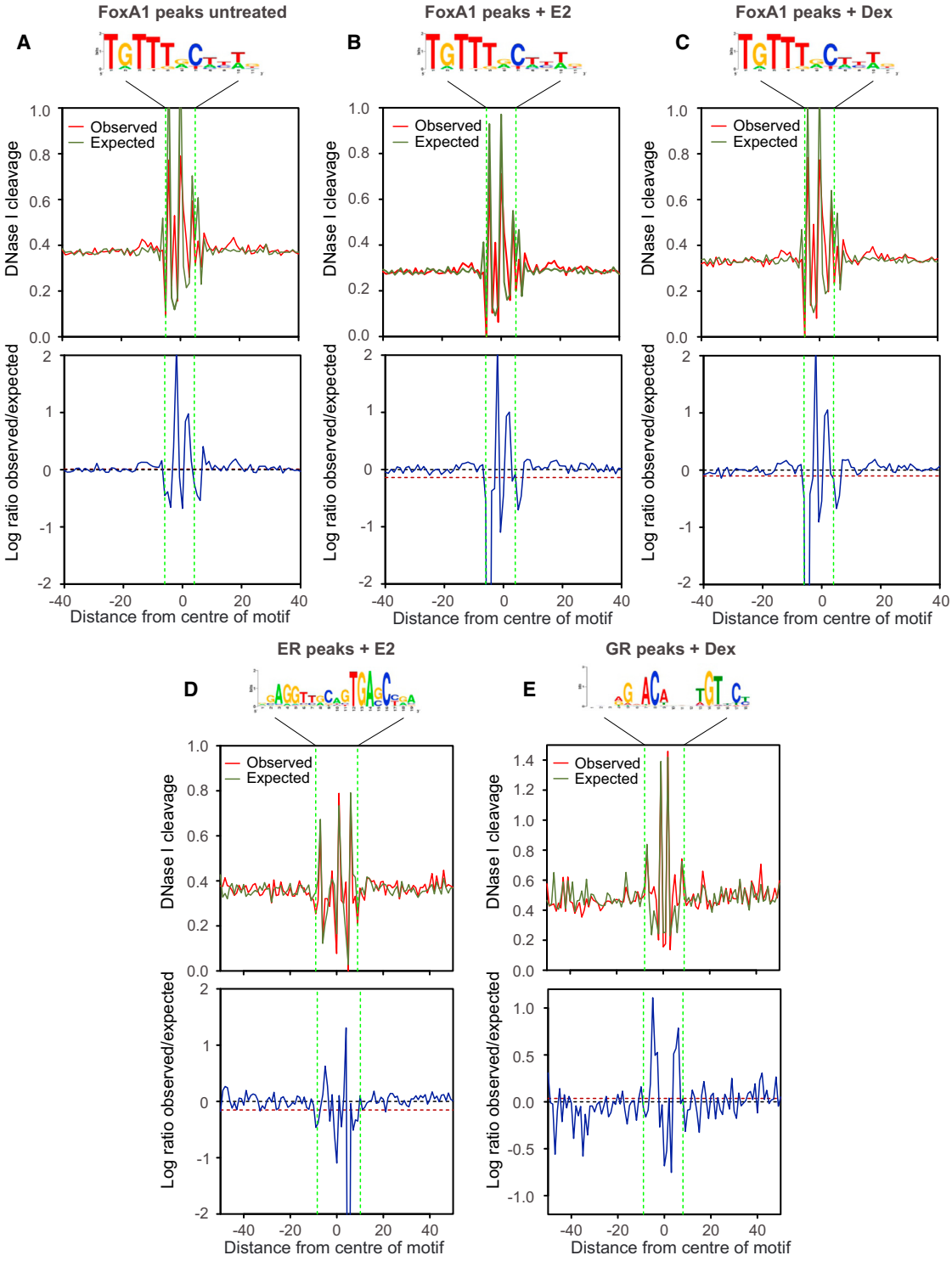

Figure 6. Lack of DHS Protection at the FoxA1 Motif Identified at FoxA1-Binding Sites in MCF-7 Breast Cancer Cells

Footprint analysis in MCF-7 cells for (A) FoxA1-untreated cells, (B) E2-treated cells, and (C) Dex-treated cells; (D) for ER treated with E2 (E); and for GR treated with Dex. The top panel represents the DNase I cleavage with the observed profile designated in red and the expected profile designated in green. The observed profiles represent the average raw DNase cut counts over the cognate motif element identified by the ChIP-seq peaks. The expected profiles represent the

(legend continued on next page)

EXPERIMENTAL PROCEDURES

Cell Culture Conditions

The MCF-7, ZR-75-1, and T-47D breast cancer cell lines have been utilized in this study. Additional description of cell culture conditions is provided in the Supplemental Experimental Procedures.

Chromatin Immunoprecipitation

ChIP experiments have been performed as per standard protocols (Kimura et al., 2008; Miranda et al., 2013). Briefly, cells were treated with either 100 nM E2 or 100 nM Dex or left untreated for 30 min. The following antibodies have been utilized: ER cocktail (Ab-10, Labvision; sc-543, Santa Cruz Biotechnology), GR (sc-1003, Santa Cruz Biotechnology), and FoxA1 (ab23738 Abcam). Two biological replicates are pooled resulting in one technical replicate. Two technical replicates per treatment group have been sequenced.

DNase I Hypersensitivity Identification

The DHS assay has been performed as previously described (John et al., 2011; Hesselberth et al., 2009). MCF-7 and ZR-75-1 cells are treated with either 100 nM E2 or 100 nM Dex or left untreated for 30 min. Two technical replicates per treatment group have been sequenced. Additional description of DHS experimental procedures is provided in the Supplemental Experimental Procedures.

Sequencing and Data Analysis

Sequence reads have been generated, and the unique tags are aligned to the human reference genome (UCSC hg19 assembly) for all ChIP- and DHS-seq data from MCF-7, ZR-75-1, and T-47D breast cancer cell lines. All sequenced data have been distributed in the GEO under GSE72252 (http://www.ncbi.nlm.nih.gov/geo/query/acc.cgi?token=mhkzgqcwzjqtbmj&acc=GSE72252.) Further description of the methods can be obtained from the Supplemental Experimental Procedures.

Analysis of DHS Footprint Signatures

Ultra deep sequencing of DHS libraries has been performed in MCF-7 and ZR-75-1 cells treated with either 100 nM E2 or 100 nM Dex or left untreated for 30 min. DHS cut count libraries have been generated as previously described (Siersbæk et al., 2014). The average DNase I cleavage of observed footprints and expected footprints and the log-ratio of observed and expected have been plotted at a bp resolution centered on the TF motif. Further description of DHS footprint analysis procedures can be obtained from the Supplemental Experimental Procedures.

Single-Molecule Tracking

The MCF-7 cells have been transiently transfected with HaloTag-FoxA1, HaloTag-ER, or HaloTag-GR to achieve appropriate protein levels for single-molecule visualization. Cells are treated with 5 nM JF_{549} HaloTag ligand (Grimm et al., 2015). MCF-7 cells are treated with either 100 nM E2 or 100 nM Dex or left untreated for 30 min, and cells are then imaged for ~2 hr at 37°C in 5% CO_2 using a custom-built microscope. Specific details and description of SMT analysis, including information on plasmid constructs, can be obtained in the Supplemental Experimental Procedures.

ACCESSION NUMBERS

The accession number for the ChIP-seq and DHS-seq data reported in this paper is GEO: GSE72252.

SUPPLEMENTAL INFORMATION

Supplemental Information includes Supplemental Experimental Procedures, six figures, and six movies and can be found with this article online at http://dx.doi.org/10.1016/j.cell.2016.02.067.

AUTHOR CONTRIBUTIONS

E.E.S. and T.B.M. performed all genome-wide experiments and prepared the manuscript. G.L.H. initiated and directed the project. V.P. and D.M.P. carried out SMT. I.G. participated in manuscript and figure preparation. T.M. and D.M. constructed the HILO microscope. T.S.K. and D.B. provided imaging instrumentation and programming support. L.G. and S.B. carried out the footprinting analysis. M.H. supported the ChIP-seq experiments. L.D.L. and J.B.G provided SMT chromophores.

ACKNOWLEDGMENTS

The authors thank the National Cancer Institute Advanced Technology Program Sequencing Facility for sequencing services. The research was supported, in part, by the Intramural Research Program of the NIH, NCI, Center for Cancer Research and the Howard Hughes Medical Institute. E.E.S. was supported, in part, by an Australian Postgraduate Award. T.B.M. was supported, in part, by a National Institute of General Medical Sciences Pharmacological Research and Training Fellowship. V.P. was supported, in part, by the Sigrid Jusélius Foundation. D.M. was supported, in part, by a Marie Curie International Incoming Fellowship (GA: 27432). T.M. was supported, in part, by the Japan Society for the Promotion of Science. L.G. was supported by the Danish Research Council and SDU2020. The authors declare the following competing financial interests: J.B.G. and L.D.L. have filed patent applications on the Janelia Fluor dyes, such as JF549, whose value may be affected by this publication.

Received: December 10, 2015
Revised: February 12, 2016
Accepted: February 25, 2016
Published: April 7, 2016

REFERENCES

Bernardo, G.M., and Keri, R.A. (2012). FOXA1: a transcription factor with parallel functions in development and cancer. Biosci. Rep. *32*, 113–130.

Biddie, S.C., John, S., Sabo, P.J., Thurman, R.E., Johnson, T.A., Schiltz, R.L., Miranda, T.B., Sung, M.H., Trump, S., Lightman, S.L., et al. (2011). Transcription factor AP1 potentiates chromatin accessibility and glucocorticoid receptor binding. Mol. Cell *43*, 145–155.

Boyle, A.P., Song, L., Lee, B.K., London, D., Keefe, D., Birney, E., Iyer, V.R., Crawford, G.E., and Furey, T.S. (2011). High-resolution genome-wide in vivo footprinting of diverse transcription factors in human cells. Genome Res. *21*, 456–464.

Caizzi, L., Ferrero, G., Cutrupi, S., Cordero, F., Ballaré, C., Miano, V., Reineri, S., Ricci, L., Friard, O., Testori, A., et al. (2014). Genome-wide activity of unliganded estrogen receptor-α in breast cancer cells. Proc. Natl. Acad. Sci. USA *111*, 4892–4897.

Caravaca, J.M., Donahue, G., Becker, J.S., He, X., Vinson, C., and Zaret, K.S. (2013). Bookmarking by specific and nonspecific binding of FoxA1 pioneer factor to mitotic chromosomes. Genes Dev. *27*, 251–260.

average of DNA hexamer frequencies from the naked DNA cut counts using the hexamers centered at each bp position. The bottom panel represents the log ratio of observed versus expected profiles. The black broken line denotes where the observed cut count levels match the expected. The red broken line is the mean of the log-ratio of observed over expected cut counts at the motif region extended by 2 bp in both directions. The difference between the black and red broken lines represents the footprint depth. See also Figure S6.

Carroll, J.S., Liu, X.S., Brodsky, A.S., Li, W., Meyer, C.A., Szary, A.J., Eeckhoute, J., Shao, W., Hestermann, E.V., Geistlinger, T.R., et al. (2005). Chromosome-wide mapping of estrogen receptor binding reveals long-range regulation requiring the forkhead protein FoxA1. Cell *122*, 33–43.

Carroll, J.S., Meyer, C.A., Song, J., Li, W., Geistlinger, T.R., Eeckhoute, J., Brodsky, A.S., Keeton, E.K., Fertuck, K.C., Hall, G.F., et al. (2006). Genome-wide analysis of estrogen receptor binding sites. Nat. Genet. *38*, 1289–1297.

Chen, J., Zhang, Z., Li, L., Chen, B.C., Revyakin, A., Hajj, B., Legant, W., Dahan, M., Lionnet, T., Betzig, E., et al. (2014). Single-molecule dynamics of enhanceosome assembly in embryonic stem cells. Cell *156*, 1274–1285.

Church, G.M., Ephrussi, A., Gilbert, W., and Tonegawa, S. (1985). Cell-type-specific contacts to immunoglobulin enhancers in nuclei. Nature *313*, 798–801.

Cirillo, L.A., Lin, F.R., Cuesta, I., Friedman, D., Jarnik, M., and Zaret, K.S. (2002). Opening of compacted chromatin by early developmental transcription factors HNF3 (FoxA) and GATA-4. Mol. Cell *9*, 279–289.

Cirillo, L.A., McPherson, C.E., Bossard, P., Stevens, K., Cherian, S., Shim, E.Y., Clark, K.L., Burley, S.K., and Zaret, K.S. (1998). Binding of the winged-helix transcription factor HNF3 to a linker histone site on the nucleosome. EMBO J. *17*, 244–254.

Eeckhoute, J., Carroll, J.S., Geistlinger, T.R., Torres-Arzayus, M.I., and Brown, M. (2006). A cell-type-specific transcriptional network required for estrogen regulation of cyclin D1 and cell cycle progression in breast cancer. Genes Dev. *20*, 2513–2526.

Galas, D.J., and Schmitz, A. (1978). DNAse footprinting: a simple method for the detection of protein-DNA binding specificity. Nucleic Acids Res. *5*, 3157–3170.

Grimm, J.B., English, B.P., Chen, J., Slaughter, J.P., Zhang, Z., Revyakin, A., Patel, R., Macklin, J.J., Normanno, D., Singer, R.H., et al. (2015). A general method to improve fluorophores for live-cell and single-molecule microscopy. Nat. Methods *12*, 244–250, 3, 250.

Grøntved, L., John, S., Baek, S., Liu, Y., Buckley, J.R., Vinson, C., Aguilera, G., and Hager, G.L. (2013). C/EBP maintains chromatin accessibility in liver and facilitates glucocorticoid receptor recruitment to steroid response elements. EMBO J. *32*, 1568–1583.

Grøntved, L., Waterfall, J.J., Kim, D.W., Baek, S., Sung, M.H., Zhao, L., Park, J.W., Nielsen, R., Walker, R.L., Zhu, Y.J., et al. (2015). Transcriptional activation by the thyroid hormone receptor through ligand-dependent receptor recruitment and chromatin remodelling. Nat. Commun. *6*, 7048.

Hager, G.L., Elbi, C., and Becker, M. (2002). Protein dynamics in the nuclear compartment. Curr. Opin. Genet. Dev. *12*, 137–141.

He, H.H., Meyer, C.A., Chen, M.W., Jordan, V.C., Brown, M., and Liu, X.S. (2012). Differential DNase I hypersensitivity reveals factor-dependent chromatin dynamics. Genome Res. *22*, 1015–1025.

He, H.H., Meyer, C.A., Hu, S.S., Chen, M.W., Zang, C., Liu, Y., Rao, P.K., Fei, T., Xu, H., Long, H., et al. (2014). Refined DNase-seq protocol and data analysis reveals intrinsic bias in transcription factor footprint identification. Nat. Methods *11*, 73–78.

Hesselberth, J.R., Chen, X., Zhang, Z., Sabo, P.J., Sandstrom, R., Reynolds, A.P., Thurman, R.E., Neph, S., Kuehn, M.S., Noble, W.S., et al. (2009). Global mapping of protein-DNA interactions in vivo by digital genomic footprinting. Nat. Methods *6*, 283–289.

Hurtado, A., Holmes, K.A., Ross-Innes, C.S., Schmidt, D., and Carroll, J.S. (2011). FOXA1 is a key determinant of estrogen receptor function and endocrine response. Nat. Genet. *43*, 27–33.

John, S., Sabo, P.J., Thurman, R.E., Sung, M.H., Biddie, S.C., Johnson, T.A., Hager, G.L., and Stamatoyannopoulos, J.A. (2011). Chromatin accessibility pre-determines glucocorticoid receptor binding patterns. Nat. Genet. *43*, 264–268.

Kassabov, S.R., Henry, N.M., Zofall, M., Tsukiyama, T., and Bartholomew, B. (2002). High-resolution mapping of changes in histone-DNA contacts of nucleosomes remodeled by ISW2. Mol. Cell. Biol. *22*, 7524–7534.

Kimura, H., Hayashi-Takanaka, Y., Goto, Y., Takizawa, N., and Nozaki, N. (2008). The organization of histone H3 modifications as revealed by a panel of specific monoclonal antibodies. Cell Struct. Funct. *33*, 61–73.

Kong, S.L., Li, G., Loh, S.L., Sung, W.K., and Liu, E.T. (2011). Cellular reprogramming by the conjoint action of ERα, FOXA1, and GATA3 to a ligand-inducible growth state. Mol. Syst. Biol. *7*, 526.

Lacroix, M., and Leclercq, G. (2004). Relevance of breast cancer cell lines as models for breast tumours: an update. Breast Cancer Res. Treat. *83*, 249–289.

Laganière, J., Deblois, G., Lefebvre, C., Bataille, A.R., Robert, F., and Giguère, V. (2005). From the cover: Location analysis of estrogen receptor alpha target promoters reveals that FOXA1 defines a domain of the estrogen response. Proc. Natl. Acad. Sci. USA *102*, 11651–11656.

Li, M., Hada, A., Sen, P., Olufemi, L., Hall, M.A., Smith, B.Y., Forth, S., McKnight, J.N., Patel, A., Bowman, G.D., et al. (2015). Dynamic regulation of transcription factors by nucleosome remodeling. eLife *4*, 4.

Lupien, M., Eeckhoute, J., Meyer, C.A., Wang, Q., Zhang, Y., Li, W., Carroll, J.S., Liu, X.S., and Brown, M. (2008). FoxA1 translates epigenetic signatures into enhancer-driven lineage-specific transcription. Cell *132*, 958–970.

McKnight, J.N., Jenkins, K.R., Nodelman, I.M., Escobar, T., and Bowman, G.D. (2011). Extranucleosomal DNA binding directs nucleosome sliding by Chd1. Mol. Cell. Biol. *31*, 4746–4759.

McNally, J.G., Müller, W.G., Walker, D., Wolford, R., and Hager, G.L. (2000). The glucocorticoid receptor: rapid exchange with regulatory sites in living cells. Science *287*, 1262–1265.

Mellor, J. (2006). Dynamic nucleosomes and gene transcription. Trends Genet. *22*, 320–329.

Miranda, T.B., Voss, T.C., Sung, M.H., Baek, S., John, S., Hawkins, M., Grøntved, L., Schiltz, R.L., and Hager, G.L. (2013). Reprogramming the chromatin landscape: interplay of the estrogen and glucocorticoid receptors at the genomic level. Cancer Res. *73*, 5130–5139.

Morisaki, T., Müller, W.G., Golob, N., Mazza, D., and McNally, J.G. (2014). Single-molecule analysis of transcription factor binding at transcription sites in live cells. Nat. Commun. *5*, 4456.

Nagaich, A.K., Walker, D.A., Wolford, R., and Hager, G.L. (2004). Rapid periodic binding and displacement of the glucocorticoid receptor during chromatin remodeling. Mol. Cell *14*, 163–174.

Nakahashi, H., Kwon, K.R., Resch, W., Vian, L., Dose, M., Stavreva, D., Hakim, O., Pruett, N., Nelson, S., Yamane, A., et al. (2013). A genome-wide map of CTCF multivalency redefines the CTCF code. Cell Rep. *3*, 1678–1689.

Rigaud, G., Roux, J., Pictet, R., and Grange, T. (1991). In vivo footprinting of rat TAT gene: dynamic interplay between the glucocorticoid receptor and a liver-specific factor. Cell *67*, 977–986.

Sekiya, T., Muthurajan, U.M., Luger, K., Tulin, A.V., and Zaret, K.S. (2009). Nucleosome-binding affinity as a primary determinant of the nuclear mobility of the pioneer transcription factor FoxA. Genes Dev. *23*, 804–809.

Siersbæk, R., Baek, S., Rabiee, A., Nielsen, R., Traynor, S., Clark, N., Sandelin, A., Jensen, O.N., Sung, M.H., Hager, G.L., and Mandrup, S. (2014). Molecular architecture of transcription factor hotspots in early adipogenesis. Cell Rep. *7*, 1434–1442.

Stenoien, D.L., Patel, K., Mancini, M.G., Dutertre, M., Smith, C.L., O'Malley, B.W., and Mancini, M.A. (2001). FRAP reveals that mobility of oestrogen receptor-alpha is ligand- and proteasome-dependent. Nat. Cell Biol. *3*, 15–23.

Sung, M.H., Guertin, M.J., Baek, S., and Hager, G.L. (2014). DNase footprint signatures are dictated by factor dynamics and DNA sequence. Mol. Cell *56*, 275–285.

Tokunaga, M., Imamoto, N., and Sakata-Sogawa, K. (2008). Highly inclined thin illumination enables clear single-molecule imaging in cells. Nat. Methods *5*, 159–161.

Voss, T.C., and Hager, G.L. (2014). Dynamic regulation of transcriptional states by chromatin and transcription factors. Nat. Rev. Genet. *15*, 69–81.

Voss, T.C., Schiltz, R.L., Sung, M.H., Yen, P.M., Stamatoyannopoulos, J.A., Biddie, S.C., Johnson, T.A., Miranda, T.B., John, S., and Hager, G.L. (2011). Dynamic exchange at regulatory elements during chromatin remodeling underlies assisted loading mechanism. Cell *146*, 544–554.

Yamaguchi, N., Ito, E., Azuma, S., Honma, R., Yanagisawa, Y., Nishikawa, A., Kawamura, M., Imai, J., Tatsuta, K., Inoue, J., et al. (2008). FoxA1 as a lineage-specific oncogene in luminal type breast cancer. Biochem. Biophys. Res. Commun. *365*, 711–717.

Yoo, A.S., and Crabtree, G.R. (2009). ATP-dependent chromatin remodeling in neural development. Curr. Opin. Neurobiol. *19*, 120–126.

Zaret, K.S., and Carroll, J.S. (2011). Pioneer transcription factors: establishing competence for gene expression. Genes Dev. *25*, 2227–2241.